ELSEVIER

Journal of Fluids and Structures 24 (2008) 1042–1057

JOURNAL OF FLUIDS AND STRUCTURES

www.elsevier.com/locate/jfs

Computation of the stress resultants of a floating Mindlin plate in response to linear wave forces

C.D. Wang*, C.M. Wang

Department of Civil Engineering, Centre for Offshore Research and Engineering, National University of Singapore, Kent Ridge, Singapore 119260, Singapore

Received 27 April 2007; accepted 19 January 2008
Available online 18 April 2008

Abstract

In this paper, we focus on the computation of stress resultants of a floating elastic plate using the Mindlin plate theory. The proposed method makes use of the linear wave theory and shallow-draft assumption. However, the usual Kirchhoff theory is replaced by the Mindlin theory for the plate. For a single frequency, the coupled water-plate problem is solved using a higher-order-coupled finite element–boundary element method. The solutions for the stress-resultants computed using the proposed method are more satisfactory than these based on the Kirchhoff plate theory.

Keywords: Hydroelastic analysis; Very large floating structures; Mindlin plate theory; FE–BE method

1. Introduction

A mat-like floating body on water where the thickness is far smaller than its length and width is usually modelled as a floating elastic plate. This is because a body with such geometry is very flexible and this results in elastic deformations due to wave forces. Examples of this type of floating elastic plate are ice floes (Squire et al., 1995) and pontoon-type very large floating structures (VLFS) (Watanabe et al., 2004). In any case, the floating elastic plate is restricted against horizontal motion but allowed to deform vertically with the waves.

The water motion is represented by its velocity potential and is solved using the linear potential theory. The plate is commonly regarded as a thin elastic plate with free-edges and zero-draft. The classical thin plate theory or Kirchhoff (1850) plate theory is commonly used to describe its motion. There are a number of ways to solve the coupled water-plate motions. To name a few, we take the example of Kashiwagi (1998) who used a combination of the pressure-distribution and mode expansion methods, where the numerical solution was given by way of B-spline functions and the Galerkin method. Another example is the method proposed by Hermans (2000) and Meylan (2002) where the boundary element method (BEM) is used to represent the velocity potential and the finite element method (FEM) for the thin plate of arbitrary geometry. Other methods are explained in detail in publications by Kashiwagi (2000) and Watanabe et al. (2004).

There are a couple of weaknesses in the conventional approaches used thus far, namely, the assumption of zero-draft and negligible thickness of the plate in the Kirchhoff theory. The former has been improved in a number of publications

*Corresponding author.
E-mail addresses: cynthia.wang@keppelom.com (C.D. Wang), cvewcm@nus.edu.sg (C.M. Wang).

0889-9746/$ - see front matter
doi:10.1016/j.jfluidstructs.2008.01.006

such as Utsunomiya et al. (1998). The improvement of the latter is the goal of this paper. The aforementioned methods (based on zero-draft) aimed primarily to determine the displacement and rarely the stress resultants. Yet the stress resultants are equally essential in checking and designing for the plate strength (e.g. the von Mises stresses in the plate). The stress resultants, however, cannot be accurately calculated using the Kirchhoff plate theory, though the displacements produced are sufficiently accurate. This inaccuracy is caused by, first, the restrictions in the Kirchhoff plate theory. This neglects the effects of transverse shear deformation and rotary inertia of the plate that become significant when the elastic wavelength is less than 20 times the thickness or when the thickness/length ratio is greater than 0.005 (Mindlin, 1951). Second, the numerical calculation of the moments and shear forces in the Kirchhoff plate is not accurate, since the stress resultants depend on the second and the third derivatives of the displacement w, where w is usually some approximation function. This inadequacy is particularly serious when FEM is employed, because of the polynomial functions used to approximate the displacement. Therefore, in order to obtain a more accurate calculation of the plate deformation, the first-order shear deformation plate theory (also known as Mindlin plate theory) is proposed. The Mindlin theory allows for the effect of transverse shear deformation and rotary inertia, and the stress resultants are expressed as, at most, first derivatives of plate displacements and rotations.

Recently, Watanabe et al. (2006) gave an analytical method to model the hydroelastic responses of a circular plate based on the Mindlin plate theory. Although it is a useful benchmarking tool, it is rather difficult to extend the method to cope with non-circular plates. For this reason, in this paper, we present a method based on the Mindlin plate theory for a rectangular plate of shallow draft. This method is an extension of the one developed by Wang and Meylan (2004), which uses a hybrid finite element–boundary element (FE–BE) method.

In this paper, the equations of plate and water motions are explained in Section 2 together with the assumptions used. In Section 3, the displacement and rotations of the plate with free-edges are solved using the FEM. These are then coupled with the integral equation of the velocity potential of the water using the linearised pressure equation that is defined on the contact surface between the plate and the water surface. Here, an interpolation of the strain functions is introduced to overcome the limitation of the chosen four-node FEM shape function. In Section 4, we present the results for the displacement and rotations of the plate. As a check, we compare the displacements computed using Mindlin and Kirchhoff plate theories as well as the moments and shear forces. We also show convergence tests for the size of elements used to discretise the plate. Finally, we present several results on displacements, moments, and shear forces.

2. Equations of plate and water motion

Although a pontoon-type floating structure on water is a three-dimensional object, we may capture its properties by considering it as a plate. In this case, we assume that the arbitrarily shaped plate covers, partially or entirely, an area of

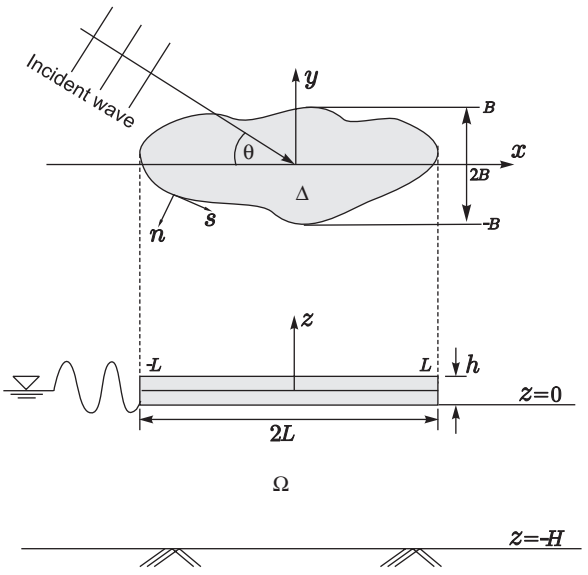

Fig. 1. Schematic diagram of the plate and the water domain.

$4LB$, has thickness h, and has no submerged part (see Fig. 1). The water underneath the plate is assumed to be an inviscid and incompressible fluid with irrotional motions such that a velocity potential exists. The water domain Ω is infinite in the x and y directions, but bounded above by the water surface $z=0$ and below by the seabed $z=-H$.

2.1. Equations of plate motion

We adopt the Mindlin plate theory to describe the plate motion. For simplicity, we shall assume that the plate is rectangular. However, the following formulation is also applicable for plates of any geometry.

The plate motion is described by the plate displacement $W(x,y;t)$ and two plate rotations $\Psi_x(x,y;t)$ and $\Psi_y(x,y;t)$. Then motion of the plate is governed by the following three simultaneous equations (Liew et al., 1998):

$$\kappa^2 Gh\left[\nabla^2 W+\frac{\partial \Psi_y}{\partial x}-\frac{\partial \Psi_x}{\partial y}\right]+\rho_p h\frac{\partial^2 W}{\partial t^2}=-\rho_w\left(\left.\frac{\partial \Phi}{\partial t}\right|_{z=0}+gW\right), \tag{1a}$$

$$D\left[\left(\frac{\partial^2 \Psi_x}{\partial y^2}-\nu\frac{\partial^2 \Psi_y}{\partial x\partial y}\right)+\frac{1-\nu}{2}\left(\frac{\partial^2 \Psi_x}{\partial x^2}-\frac{\partial^2 \Psi_y}{\partial x\partial y}\right)\right]+\kappa^2 Gh\left(\frac{\partial W}{\partial y}-\Psi_x\right)+\rho_p\frac{h^3}{12}\frac{\partial^2 \Psi_x}{\partial t^2}=0, \tag{1b}$$

$$D\left[\left(\frac{\partial^2 \Psi_y}{\partial x^2}-\nu\frac{\partial^2 \Psi_x}{\partial x\partial y}\right)+\frac{1-\nu}{2}\left(\frac{\partial^2 \Psi_y}{\partial y^2}-\frac{\partial^2 \Psi_x}{\partial x\partial y}\right)\right]-\kappa^2 Gh\left(\frac{\partial W}{\partial x}-\Psi_y\right)+\rho_p\frac{h^3}{12}\frac{\partial^2 \Psi_y}{\partial t^2}=0, \tag{1c}$$

where $\Phi(x,y,z;t)$ is the linear velocity potential of the water, ρ_w the water density, ρ_p the plate density, $G=E/[2(1+\nu)]$ the shear modulus, $D=Eh^3/[12(1-\nu^2)]$ the flexural rigidity, E the modulus of elasticity, ν the Poisson ratio, and κ^2 the shear correction factor. Note that as the thickness h becomes small, the terms $\Psi_x\to\partial W/\partial y$ and $\Psi_y\to\partial W/\partial x$ and the governing equations of motion reduce to that of the classical thin plate theory when the rotary inertia terms are neglected as well.

The free-edge boundary conditions state that the bending and twisting moments and the shear forces must vanish at the edges of the plate. Therefore,

$$M_{nn}=0,\quad M_{ns}=0,\quad Q_n=0, \tag{2}$$

where M_{nn} and M_{ns} are the bending and twisting moments given by

$$M_{nn}=D\left(\frac{\partial \Psi_s}{\partial n}-\nu\frac{\partial \Psi_n}{\partial s}\right),\quad M_{ns}=\frac{D(1-\nu)}{2}\left(\frac{\partial \Psi_s}{\partial s}-\frac{\partial \Psi_n}{\partial n}\right) \tag{3a,b}$$

and Q_n is the shear force given by

$$Q_n=\kappa^2 Gh\left(\frac{\partial W}{\partial n}-\Psi_s\right), \tag{4}$$

with $n(x,y)$ and $s(x,y)$ being, respectively, the normal and tangential directions to the edges of the plate.

2.1.1. Nondimensionalisation

We nondimensionalise the spatial variables with respect to characteristic length L and time variables with respect to $\sqrt{L/g}$ such that

$$x=L\bar{x},\quad y=L\bar{y},\quad z=L\bar{z},\quad W=L\bar{W} \tag{5a}$$

and

$$t=\sqrt{\frac{L}{g}}\bar{t},\quad \Phi=L\sqrt{Lg}\bar{\Phi}. \tag{5b}$$

Note that Ψ_x and Ψ_y are the plate rotations and hence they are dimensionless.

2.1.2. Reduction to single frequency problem

We now consider the problem at a single frequency which allows us to represent the time-dependence by $\exp(-\mathrm{i}\omega\bar{t})$, where ω is the dimensionless angular frequency. Thus the displacement, the rotations and the potential can be written as

$$\bar{W}(\bar{x},\bar{y};\bar{t})=w(\bar{x},\bar{y})\mathrm{e}^{-\mathrm{i}\omega\bar{t}},\quad \bar{\Psi}_x(\bar{x},\bar{y};\bar{t})=\psi_x(\bar{x},\bar{y})\mathrm{e}^{-\mathrm{i}\omega\bar{t}},\quad \bar{\Psi}_y(\bar{x},\bar{y};\bar{t})=\psi_y(\bar{x},\bar{y})\mathrm{e}^{-\mathrm{i}\omega\bar{t}}$$

and

$$\Phi(\bar{x},\bar{y},\bar{z};\bar{t}) = \phi(\bar{x},\bar{y},\bar{z})\mathrm{e}^{-\mathrm{i}\omega\bar{t}}.$$

Therefore Eqs. (1a)–(1c) become

$$\beta\frac{6\kappa^2(1-\nu)}{\bar{h}^2}\left[\nabla^2 w + \frac{\partial\psi_y}{\partial\bar{x}} - \frac{\partial\psi_x}{\partial\bar{y}}\right] - \omega^2\gamma_1 w = \mathrm{i}\omega\phi - w, \tag{6a}$$

$$\beta\left\{\left[\left(\frac{\partial^2\psi_x}{\partial\bar{y}^2} - \nu\frac{\partial^2\psi_y}{\partial\bar{x}\partial\bar{y}}\right) + \frac{1-\nu}{2}\left(\frac{\partial^2\psi_x}{\partial\bar{x}^2} - \frac{\partial^2\psi_y}{\partial\bar{x}\partial\bar{y}}\right)\right] + \frac{6\kappa^2(1-\nu)}{\bar{h}^2}\left(\frac{\partial w}{\partial\bar{y}} - \psi_x\right)\right\} - \omega^2\gamma_2\psi_x = 0, \tag{6b}$$

$$\beta\left\{\left[\left(\frac{\partial^2\psi_y}{\partial\bar{x}^2} - \nu\frac{\partial^2\psi_x}{\partial\bar{x}\partial\bar{y}}\right) + \frac{1-\nu}{2}\left(\frac{\partial^2\psi_y}{\partial y^2} - \frac{\partial^2\psi_x}{\partial\bar{x}\partial\bar{y}}\right)\right] - \frac{6\kappa^2(1-\nu)}{\bar{h}^2}\left(\frac{\partial w}{\partial\bar{x}} - \psi_y\right)\right\} - \omega^2\gamma_2\psi_y = 0, \tag{6c}$$

where β, γ_1, and γ_2 are dimensionless variables given by Tayler (1986)

$$\beta = \frac{D}{\rho_w g L^4}, \quad \gamma_1 = \frac{\rho_p h}{\rho_w L}, \quad \gamma_2 = \frac{\rho_p h^3}{12\rho_w L^3} = \frac{\bar{h}^2}{12}\gamma_1. \tag{7}$$

Thereafter, we drop the overbar for simplicity.

2.2. Equations of water motion

Following Stoker (1957) and Wehausen and Laitone (1960), the velocity potential of the water $\phi(\mathbf{x},z)$ is described by the Laplace equation

$$\nabla^2\phi = 0, \quad (\mathbf{x},z) \in \Omega, \tag{8}$$

with boundary conditions

$$\frac{\partial\phi}{\partial z} = \omega^2\phi, \quad \mathbf{x}\notin\Delta, \ z = 0, \tag{9}$$

$$\left.\begin{array}{ll}\dfrac{\partial\phi}{\partial z} = 0, & -\infty<\mathbf{x}<\infty, z=-H,\\ \nabla\phi\to 0, & -\infty<\mathbf{x}<\infty, \ z\to-\infty,\end{array}\right\} \tag{10}$$

where $\mathbf{x} = (x,y)$.

At infinity, the boundary condition is given by the Sommerfeld radiation condition (Wehausen and Laitone, 1960)

$$\lim_{|\mathbf{x}|\to\infty}\sqrt{|\mathbf{x}|}\left(\frac{\partial}{\partial|\mathbf{x}|} - \mathrm{i}k\right)(\phi - \phi^{\mathrm{In}}) = 0, \tag{11}$$

where $\phi^{\mathrm{In}}(\mathbf{x},z)$ is the incident potential which is the solution of boundary value problem posed by Eqs. (8)–(10). At $z = 0$, the incident wave is given by

$$\phi^{\mathrm{In}}(\mathbf{x}) = \frac{A}{\omega}\mathrm{e}^{\mathrm{i}k(x\cos\theta + y\sin\theta)}, \tag{12}$$

with A the dimensionless wave amplitude and θ the angle of incidence. The wavenumber k is related to the wavelength λ by

$$\lambda = \frac{2\pi}{k} \tag{13}$$

and to the frequency ω by the dimensionless dispersion equation

$$\omega^2 = k\tanh(kH), \tag{14}$$

where, as $H\to\infty$, we obtain

$$\omega^2 = k. \tag{15}$$

Conventionally, the linear wave potential $\phi(x,y,z)$ is solved using the BEM. This is done by transforming Laplace equation (8) with boundary conditions (9)–(11) into an integral equation involving a free-surface Green's function. The resulting integral equation is

$$\phi(\mathbf{x}) = \phi^{\mathrm{In}}(\mathbf{x}) + \int_{\Delta} G(\mathbf{x};\boldsymbol{\xi})[\omega^2\phi(\boldsymbol{\xi}) + \mathrm{i}\omega w(\boldsymbol{\xi})]\,\mathrm{d}\boldsymbol{\xi}, \tag{16}$$

where $\boldsymbol{\xi} = (\xi,\eta)$ and $G(\mathbf{x};\boldsymbol{\xi})$ is a free surface Green's function given by

$$G(\mathbf{x};\boldsymbol{\xi}) = -\sum_{j=0}^{\infty} \frac{\mathrm{K}_0(k_j|\mathbf{x}-\boldsymbol{\xi}|)}{2\pi C_j}\cos^2(k_j H), \tag{17}$$

if $z=-H$ (Wehausen and Laitone, 1960; Mei, 1982; Linton, 1999) and

$$G(\mathbf{x};\boldsymbol{\xi}) = \frac{1}{4\pi}\left\{\frac{2}{|\mathbf{x}-\boldsymbol{\xi}|} - \pi\omega^2[\mathrm{H}_0(\omega^2|\mathbf{x}-\boldsymbol{\xi}|) + \mathrm{Y}_0(\omega^2|\mathbf{x}-\boldsymbol{\xi}|) - 2\mathrm{i}\mathrm{J}_0(\omega^2|\mathbf{x}-\boldsymbol{\xi}|)]\right\}, \tag{18}$$

if $z=-H\to-\infty$ (Wehausen and Laitone, 1960). In Eq. (18), H_0, J_0, and Y_0 are, respectively, the Struve function, the first kind, and the second kind Bessel functions where all are of order zero. In Eq. (17), K_0 is the second kind modified Bessel function (Abramowitz and Stegun, 1964) and k_j are the roots of the dispersion equation that are related to the angular frequency by equation

$$-k_j\tan(k_j H) = \omega^2, \quad j>0. \tag{19}$$

If $j=0$, from Eq. (14), k_0 clearly becomes $k_0 = \mathrm{i}k$, where k is the wavenumber. The constants C_j are given by

$$C_j = \frac{H}{2}\left(1 + \frac{\sin 2k_j H}{2k_j H}\right). \tag{20}$$

3. Numerical solution

3.1. Application of Finite Element Method

A variational equation equivalent to Eqs. (6a)–(6c) is given by the Hamiltonian principle involving the plate energy functionals (Liew et al., 1998); that is

$$\delta\int_{t_0}^{t_f}(U - T + W)\,\mathrm{d}t = 0. \tag{21}$$

The potential energy function U and the kinetic energy function T are, respectively, given by

$$U = \frac{1}{2}\int_{\Delta}(\{\varepsilon\}^{\mathrm{T}}[B^f]\{\varepsilon\} + \{\gamma\}^{\mathrm{T}}[B^s]\{\gamma\})\,\mathrm{d}\mathbf{x}, \tag{22}$$

$$T = \frac{1}{2}\omega^2\int_{\Delta}[\gamma_1 w^2 + \gamma_2(\psi_x^2 + \psi_y^2)]\,\mathrm{d}\mathbf{x} \tag{23}$$

and the work done W is given by

$$W = \int_{\Delta} w\left(\mathrm{i}\omega\phi - \frac{1}{2}w\right)\mathrm{d}\mathbf{x}. \tag{24}$$

In Eq. (22), the $\{\varepsilon\}$ and $\{\gamma\}$ represent the plate's section curvature and shearing strain, respectively (Bathe and Dvorkin, 1985),

$$\{\varepsilon\} = \begin{Bmatrix} \dfrac{\partial\psi_y}{\partial x} \\ -\dfrac{\partial\psi_x}{\partial y} \\ \dfrac{\partial\psi_y}{\partial y} - \dfrac{\partial\psi_x}{\partial x} \end{Bmatrix}, \quad \{\gamma\} = \begin{Bmatrix} \dfrac{\partial w}{\partial x} + \psi_y \\ \dfrac{\partial w}{\partial y} - \psi_x \end{Bmatrix}; \tag{25}$$

while matrices $[B^f]$ and $[B^s]$ are

$$[B^f] = \beta \begin{bmatrix} 1 & v & 0 \\ v & 1 & 0 \\ 0 & 0 & \dfrac{1-v}{2} \end{bmatrix}, \quad [B^s] = 6\beta \frac{\kappa^2(1-v)}{\bar{h}^2} \begin{bmatrix} 1 & 0 \\ 0 & 1 \end{bmatrix}. \tag{26a,b}$$

Since we have assumed that the problem is solved for a single frequency, Eq. (21) becomes

$$\begin{aligned} &\frac{1}{2}\,\delta \int_{\Delta} \beta \left\{ \left[\left(\frac{\partial \psi_y}{\partial x}\right)^2 + \left(\frac{\partial \psi_x}{\partial y}\right)^2 - 2v \frac{\partial \psi_x}{\partial y}\frac{\partial \psi_y}{\partial x} + \frac{1-v}{2}\left(\frac{\partial \psi_y}{\partial y} - \frac{\partial \psi_x}{\partial x}\right)^2 \right] \right. \\ &\left. + \frac{6\kappa^2(1-v)}{\bar{h}^2} \left[\left(\frac{\partial w}{\partial x} + \psi_y\right)^2 + \left(\frac{\partial w}{\partial y} - \psi_x\right)^2 \right] \right\} \mathrm{d}\mathbf{x} - \frac{1}{2}\,\omega^2 \delta \int_{\Delta} \{\gamma_1 w^2 + \gamma_2[(\psi_x)^2 + (\psi_x)^2]\}\,\mathrm{d}\mathbf{x} \\ &\quad = \mathrm{i}\omega\delta \int_{\Delta} \phi w\,\mathrm{d}\mathbf{x} - \frac{1}{2}\,\delta \int_{\Delta} w^2\,\mathrm{d}\mathbf{x}. \end{aligned} \tag{27}$$

Following the FEM, we discretise the plate using p rectangular elements which each has area of $4ab$. Then we approximate the displacement w and rotations ψ_x and ψ_y using a set of polynomials χ_j such that

$$w = \sum_{d=1}^{p} \chi_d(\mathbf{x}) \hat{w}_d, \quad \psi_x = \sum_{d=1}^{p} \chi_d(\mathbf{x}) \hat{\psi}_{x,d}, \quad \psi_y = \sum_{d=1}^{p} \chi_d(\mathbf{x}) \hat{\psi}_{y,d}. \tag{28}$$

Similarly, we also approximate the potentials ϕ_{in} and ϕ using the same set of polynomials χ_j

$$\phi^{\mathrm{In}} = \sum_{d=1}^{p} \chi_d(\mathbf{x})\, \hat{\phi}_d^{\,\mathrm{In}}, \quad \phi = \sum_{d=1}^{p} \chi_d(\mathbf{x})\, \hat{\phi}_d, \tag{29}$$

where χ_d is related to the FEM basis functions N_i by

$$\chi_d(\mathbf{x}) = \sum_{i=1}^{q_d} o_{di}\, N_i(\mathbf{x}). \tag{30}$$

The constants o_{di} weigh element Δ_d, which encloses $\mathbf{x}$, with respect to the plate (Wang and Meylan, 2004). The summation is taken over the number of nodes q_d in element Δ_d where the shape function N_i is defined. We choose shape function N_i to be the linear serendipity function which is defined at four corners (nodes) of the element Zienkiewicz (1977),

$$N_i(\mathbf{x}) = (1 + \xi_i\xi)(1 + \eta_i\eta), \quad i = 1, \ldots, 4, \tag{31}$$

where $(\xi, \eta) = (x/a, y/b)$ for a rectangular element of area $4ab$ and (ξ_i, η_i) is the coordinate of the ith node of Δ_d. Moreover, for p rectangular elements that discretize the plate, we have a total of q nodes. Constants $\hat{w}_d$, $\hat{\psi}_{x,d}$, and $\hat{\psi}_{y,d}$ are, respectively, the displacement and rotations of the nodes of element d (Wang and Meylan, 2004). Note that the aforementioned formulation can easily be extended to arbitrary quadrilateral elements with corresponding shape functions.

3.2. Solution for coupled plate-water motion

We minimise Eq. (27) with respect to $\hat{w}_e$, $\psi_{x,e}$, and $\psi_{y,e}$ and solve the resulting equations locally for each element Δ_d. By taking $\mathbf{x}$ to correspond to the nodes of the plate we arrive at

$$\{\beta(\mathbb{K}^f + \mathbb{K}^s) + \mathbb{M}^* - \omega^2 \mathbb{M}\}\hat{\mathbf{w}} = \mathrm{i}\omega \mathbb{M}^* \hat{\phi}, \tag{32}$$

where

$$\mathbb{K}^s = \sum_{d=1}^{p} [o]_d^{\mathrm{T}} [k^s]_d [o]_d, \quad \mathbb{K}^f = \sum_{d=1}^{p} [o]_d^{\mathrm{T}} [k^f]_d [o]_d \tag{33}$$

and

$$\mathbb{M} = \sum_{d=1}^{p} [o]_d^{\mathrm{T}} [m]_d [o]_d, \quad \mathbb{M}^* = \sum_{d=1}^{p} [o]_d^{\mathrm{T}} [m^*]_d [o]_d, \tag{34}$$

$$\hat{\mathbf{w}} = \sum_{d=1}^{p} [o]_d^{\mathrm{T}} [\hat{w}]_d, \quad \hat{\phi} = \sum_{d=1}^{p} [o]_d^{\mathrm{T}} [\hat{\phi}]_d. \tag{35}$$

Matrices $\mathbb{K}^f$ and $\mathbb{K}^s$ are, the stiffness matrices due to flexure and shear, respectively. Matrices $\mathbb{M}$ and $\mathbb{M}^*$ are the mass matrices. Vector $\hat{\phi}$ represents the force exerted upon the plate by water where it satisfies the following equation:

$$\mathbb{M}^* \hat{\phi} = \mathbb{M}^* \hat{\phi}^{\mathrm{In}} + \omega^2 \mathbb{G} \hat{\phi} + \mathrm{i}\omega \mathbb{G} \hat{\mathbf{w}}, \tag{36}$$

where $\mathbb{G}$ is the Green matrix containing the free-surface Green's function as defined by Eqs. (17) and (18) and is given by Wang and Meylan (2004)

$$\mathbb{G} = \sum_{d=1}^{p} \sum_{e=1}^{p} [o]_d^{\mathrm{T}} [g]_{de} [o]_e. \tag{37}$$

All matrices are of dimension $3q \times 3q$ and each is composed of 12×12 elemental matrices. Constant vector $[\hat{w}]_d$ contains the nodal displacement and rotations and has the form

$$\{\hat{w}\}_d^{\mathrm{T}} = \{w_1, \psi_{x,1}, \psi_{y,1}, w_2, \psi_{x,2}, \psi_{y,2}, w_3, \psi_{x,3}, \psi_{y,3}, w_4, \psi_{x,4}, \psi_{y,4}\}^{\mathrm{T}}, \tag{38}$$

with dimension $3q \times 1$. Vector $[\hat{\phi}]$ contains the potential defined at each node and is given by

$$\{\hat{\phi}\}_d^{\mathrm{T}} = \{\phi_1, 0, 0, \phi_2, 0, 0, \phi_3, 0, 0, \phi_4, 0, 0\}^{\mathrm{T}}. \tag{39}$$

The assembling matrix $[o]_d$ is given in Wang and Meylan (2004).

With the exception of $[k^s]_d$, the elemental matrices $[k^f]_d$, $[m^*]_d$, $[m]_d$, and $[g]_{de}$ follow the standard FEM procedure as given by Zienkiewicz (1977) and Wang and Meylan (2004). Each 3×3 submatrix of $[k^f]_d, [m^*]_d$, $[m]_d$, and $[g]_{de}$ are given by

$$[k_{ij}^f]_d = \int_{\Delta_d} \begin{bmatrix} 0 & 0 & 0 \\ 0 & \dfrac{\partial N_i}{\partial x}\dfrac{\partial N_j}{\partial x} + \dfrac{1-v}{2}\dfrac{\partial N_i}{\partial y}\dfrac{\partial N_j}{\partial y} & -\left(v\dfrac{\partial N_i}{\partial x}\dfrac{\partial N_j}{\partial y} + \dfrac{1-v}{2}\dfrac{\partial N_i}{\partial y}\dfrac{\partial N_j}{\partial x}\right) \\ 0 & -\left(v\dfrac{\partial N_i}{\partial y}\dfrac{\partial N_j}{\partial x} + \dfrac{1-v}{2}\dfrac{\partial N_i}{\partial x}\dfrac{\partial N_j}{\partial y}\right) & \dfrac{\partial N_i}{\partial y}\dfrac{\partial N_j}{\partial y} + \dfrac{1-v}{2}\dfrac{\partial N_i}{\partial x}\dfrac{\partial N_j}{\partial x} \end{bmatrix} \mathrm{d}\mathbf{x}, \tag{40}$$

$$[m_{ij}]_d = \int_{\Delta_d} \begin{bmatrix} \gamma_1 N_i N_j & & \\ & \gamma_2 N_i N_j & \\ & & \gamma_2 N_i N_j \end{bmatrix} \mathrm{d}\mathbf{x}, \quad [m_{ij}^*]_d = \int_{\Delta_d} \begin{bmatrix} N_i N_j & & \\ & 0 & \\ & & 0 \end{bmatrix} \mathrm{d}\mathbf{x} \tag{41a,b}$$

and

$$[g_{ij}]_{de} = \int_{\Delta_d} \int_{\Delta_e} \begin{bmatrix} N_i(\mathbf{x}_d) G(\mathbf{x}_d; \boldsymbol{\xi}_e) N_j(\boldsymbol{\xi}_e) & & \\ & 0 & \\ & & 0 \end{bmatrix} \mathrm{d}\boldsymbol{\xi}\, \mathrm{d}\mathbf{x}, \tag{42}$$

where $i,j = 1, \ldots, 4$ and (x_d) and (ξ_e) correspond, respectively, to source panel Δ_d and field panel Δ_e. We integrate Eqs. (40), (41a,b) exactly, while the integrations over elements Δ_d and Δ_e in Eq. (42) are solved using the Gauss–Legendre quadrature (Wang and Meylan, 2004). Notice that $[k^f]_d$ is derived from the product involving $\{\varepsilon\}$ in Eq. (22) while $[m]_d$ comes from the kinetic energy functional T in Eq. (23) and $[m^*]_d$ and $[g]_{de}$ are from W in Eq. (24). However, $[k^s]_d$ will not be derived directly from the product of $\{\gamma\}$ in Eq. (22). This will be discussed in the next part.

3.2.1. Computation of stiffness matrix due to shear

Submatrix $[k^s]_d$ must be computed differently due to a common problem encountered when using the four-node elements in the computation of the transverse shear strains of a Mindlin plate. The reason is that the approximation of Eq. (28) with the given shape function, given by Eq. (31), in Eq. (48) is inaccurate as $h \to 0$ because the four-node element discretisation is unable to capture the vanishing transverse shear strains at the edges of the plate despite the fact that Eq. (27) contains Kirchhoff's thin plate formulation (Bathe and Dvorkin, 1985; Zienkiewicz, 1977). To resolve this problem, we follow the method developed by Bathe and Dvorkin (1985).

Instead of computing $[k^s]_d$ directly from $\{\gamma\}$ in Eq. (22) or the second term of Eq. (27), we interpolate the shear strain on individual elements and use an approximation. The interpolation is done in the following way. First, we define the nodes of an element, say Δ_d, to be $q_1^{(d)} = (-1,-1)$, $q_2^{(d)} = (-1,1)$, $q_3^{(d)} = (1,-1)$ and $q_4^{(d)} = (1,1)$, as shown in Fig. 2. We

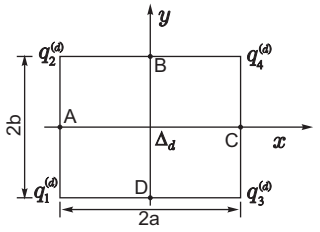

Fig. 2. Diagram of panel.

also define a set of mid-points A, B, C, and D at, respectively $(-1,0)$, $(0,1)$, $(1,0)$, and $(0,-1)$. Then, using the definition of $\{\gamma\}$ in Eq. (25), the shear strain at an arbitrary point X enclosed by Δ_d is given by

$$\gamma_{xz}^{(X)} = \left.\frac{\partial w}{\partial x}\right|_X + \psi_y|_X, \quad \gamma_{yz}^{(X)} = \left.\frac{\partial w}{\partial y}\right|_X - \psi_x|_X, \tag{43}$$

where $\partial w/\partial x$, $\partial w/\partial y$, ψ_x, and ψ_y are approximated using Eq. (28).

Next we introduce the following interpolations for $\gamma_{xz}^{(X)}$ and $\gamma_{yz}^{(X)}$ using the components of Eq. (43):

$$\{\gamma\} = \begin{Bmatrix} \gamma_{xz} \\ \gamma_{yz} \end{Bmatrix} = \begin{Bmatrix} \frac{1}{2}(1+\eta)\gamma_{xz}^B + \frac{1}{2}(1-\eta)\gamma_{xz}^D \\ \frac{1}{2}(1-\xi)\gamma_{yz}^A + \frac{1}{2}(1+\xi)\gamma_{yz}^C \end{Bmatrix}, \tag{44}$$

where γ_{yz}^A, γ_{xz}^B, γ_{yz}^C, and γ_{xz}^D are computed using Eq. (43) and $(\xi,\eta) = (x/a, y/b)$. By substituting Eq. (43) into Eq. (44), we obtain

$$\begin{Bmatrix} \gamma_{xz} \\ \gamma_{yz} \end{Bmatrix} = \begin{Bmatrix} \frac{1}{2}(1+\eta)\left[\frac{w_4 - w_2}{2} + \frac{\psi_{y,4} + \psi_{y,2}}{2}\right] + \frac{1}{2}(1-\eta)\left[\frac{w_3 - w_1}{2} + \frac{\psi_{y,3} + \psi_{y,1}}{2}\right] \\ \frac{1}{2}(1-\xi)\left[\frac{w_2 - w_1}{2} + \frac{\psi_{x,2} + \psi_{x,1}}{2}\right] + \frac{1}{2}(1+\xi)\left[\frac{w_4 - w_3}{2} + \frac{\psi_{x,4} + \psi_{x,3}}{2}\right] \end{Bmatrix}. \tag{45}$$

Using the standard FEM procedure, we may write Eq. (45) as

$$\{\gamma\} = [c^s]\{\hat{w}\}_d, \tag{46}$$

where $\{\hat{w}\}_d$ is given in Eq. (38) and the 2×12 matrix $[c^s]$ is given by

$$[c^s]^{\mathrm{T}} = \frac{1}{4}\begin{bmatrix} -(1-\eta) & -(1-\xi) \\ 0 & -(1-\xi) \\ 1-\eta & 0 \\ -(1+\eta) & 1-\xi \\ 0 & -(1-\xi) \\ 1+\eta & 0 \\ 1-\eta & -(1+\xi) \\ 0 & -(1+\xi) \\ 1-\eta & 0 \\ 1+\eta & 1+\xi \\ 0 & -(1+\xi) \\ 1+\eta & 0 \end{bmatrix}^{\mathrm{T}}. \tag{47}$$

Using Eqs. (46) and (47), we may write the stiffness matrix due to shear $[k^s]_d$ as

$$[k^s]_d = \int_{\Delta_d} [c^s]^{\mathrm{T}}[B^s][c^s]\,\mathrm{d}\mathbf{x}, \tag{48}$$

where $[B^s]$ is given in Eq. (26b).

3.2.2. Inversion of the Green matrix

We can solve simultaneous Eqs. (36) and (32) for either $\hat{\mathbf{w}}$ and $\hat{\phi}$. In order to solve for $\hat{\mathbf{w}}$, we substitute Eq. (36) into Eq. (32) and obtain the linear equation

$$\{\beta[\mathbb{K}^f + \mathbb{K}^s] + [\mathbb{M}^* - \omega^2\mathbb{M}] + \mathbb{M}^*(\mathbb{M}^* - \omega^2\mathbb{G})^{-1}\mathbb{G}\}\hat{\mathbf{w}} = \mathrm{i}\omega\mathbb{M}^*(\mathbb{M}^* - \omega^2\mathbb{G})^{-1}\mathbb{M}^*\hat{\phi}^{\mathrm{In}}. \tag{49}$$

We notice from Eq. (16) (which corresponds to Eq. (36)) that the Green's function is only applied to the displacement w and ϕ. Therefore, in the computation of Eq. (49), matrices $\mathbb{M}^*$ and $\mathbb{G}$ are non-zero only on the components that correspond to w and ϕ of the nodes. Moreover, the location of these non-zero entries are the same for both matrices. The result of computing $[\mathbb{M}^* - \omega^2\mathbb{G}]$ is a matrix with non-zero entries at $(3m-2, 3n-2)$ for $m, n = 1 \ldots q$. To invert this, we use transformation matrices to obtain an upper left matrix, which we can invert. This method can be found in textbooks such as Landesman and Hestenes (1992).

First, we introduce a permutation $3q \times 3q$ matrix $\mathbb{P}$, with non-zero entries located at $(m, 3n-2)$, that transforms $[\mathbb{M}^* - \omega^2\mathbb{G}]$ into an upper left matrix $[\mathbb{P}(\mathbb{M}^* - \omega^2\mathbb{G})\mathbb{P}^{\mathrm{T}}]$. Then, this upper left matrix is transformed into a full matrix $\tilde{\mathbb{G}}$ by the following equation:

$$\tilde{\mathbb{G}} = \mathbb{U}^{\mathrm{T}}\mathbb{P}(\mathbb{M}^* - \omega^2\mathbb{G})\mathbb{P}^{\mathrm{T}}\mathbb{U}, \tag{50}$$

where $\mathbb{U}$ is a matrix with columns containing the basis of the range of $(\mathbb{M} - \omega^2\mathbb{G})$ (Landesman and Hestenes, 1992). Finally, since $\tilde{\mathbb{G}}$ is invertible, we can obtain the inverse of $[\mathbb{M}^* - \omega^2\mathbb{G}]$ by applying the permutation matrix $\mathbb{P}$ to $\tilde{\mathbb{G}}^{-1}$. This gives us

$$(\mathbb{M}^* - \omega^2\mathbb{G})^{-1} = \mathbb{P}^{\mathrm{T}}\tilde{\mathbb{G}}^{-1}\mathbb{P}. \tag{51}$$

4. Results

4.1. Convergence study

Before we begin validating the present method, we first show that the natural frequencies of a plate with free-edges agree with known results (Liu et al., 1991; Liew et al., 1993). The natural frequencies of a Kirchhoff plate are obtained by solving the following eigenfunction equation:

$$\mathbb{K}\hat{\mathbf{w}}_i = \lambda_i\mathbb{M}\hat{\mathbf{w}}_i, \tag{52}$$

where $\lambda_i = \omega^2(\gamma_1/\beta)$ and matrices $\mathbb{K}$ and $\mathbb{M}$ are the stiffness and the mass matrix corresponding to a Kirchhoff plate, respectively. Similarly, the eigenfunction equation for a Mindlin plate is

$$(\mathbb{K}^f + \mathbb{K}^s)\hat{\mathbf{w}}_i = \lambda_i\mathbb{M}\hat{\mathbf{w}}_i, \tag{53}$$

where $\mathbb{K}^f$, $\mathbb{K}^s$, and $\mathbb{M}$ are given in Eqs. (33) and (34).

For natural frequencies $\sqrt{\lambda_i}$, we use a square plate of area 1 and vary the thickness h to follow Liu et al. (1991). The results for the case $v = 0.3$ are given in Table 1 where the Kirchhoff plate is discretised using 100 elements and the Mindlin plate is discretised using 900 elements, since we use fourth order elements for Kirchhoff solution and linear elements for the Mindlin solution. Results for the Kirchhoff plate agree with those by Liu et al. (1991) for a freely vibrating plate. Results for the Mindlin analysis agree with those by Liew et al. (1993) (note that the cited frequencies are multiplied by π^2).

Table 1
Comparison of the first four non-zero natural frequencies $\sqrt{\lambda_i}$ of a Kirchhoff and a Mindlin plate for different plate thicknesses

$\sqrt{\lambda_i}$	Kirchhoff	Mindlin		
		$h = 1/100$	$h = 1/10$	$h = 1/5$
$i = 1$	13.4738	13.0087	12.7128	11.3738
$i = 2$	19.6024	19.1400	18.8977	16.9228
$i = 3$	24.2835	24.4395	23.8492	21.3645
$i = 4$	34.8010	33.6219	31.2146	27.0614

Next, we compare the results of the present method (denoted by method M) with those computed using the higher-order FE–BE-Kirchhoff plate method (denoted by method K) by Wang and Meylan (2004). For the comparison, a square plate of area 16, $h = 0.01$, $\beta = 0.01$, and $\gamma_1 = h$, $\gamma_2 = \frac{1}{12}h^2\gamma_1$ on water of infinite depth is used. The wavelength is $\lambda = 2$ and the waveangle is $\theta = \pi/4$. The shear correction factor κ^2 is taken to be $\frac{5}{6}$ and the Poisson ratio is $v = 0.3$. We use 900 elements for method M whereas method K uses 100 elements. Fig. 3 shows the displacement of the plate (w/A) calculated using methods M and K. The displacement calculated using method M is slightly larger in magnitude than

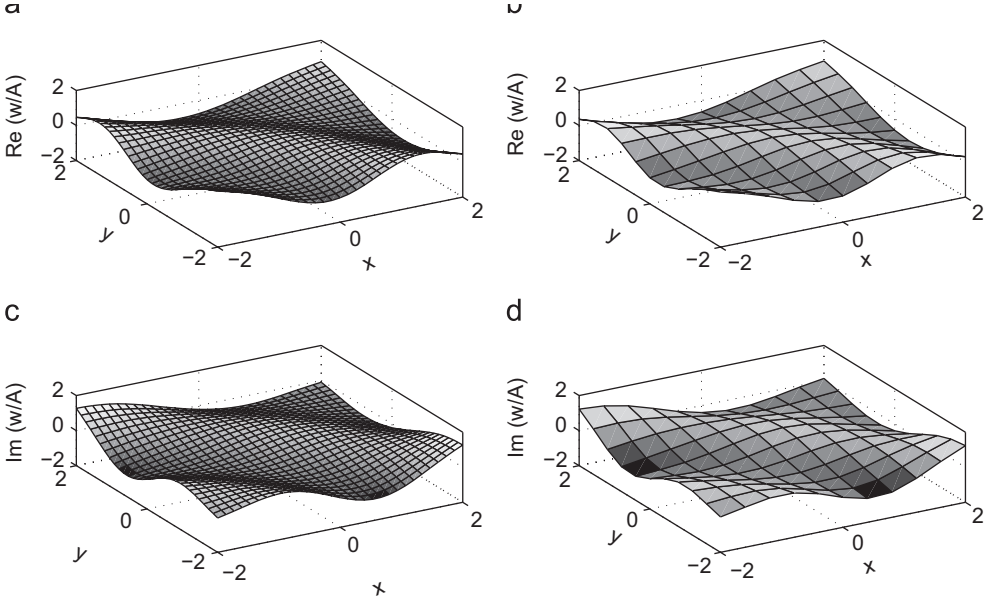

Fig. 3. Comparison of real (1st row) and imaginary part (2nd row) of the plate displacement calculated using method M (left) and method K (right).

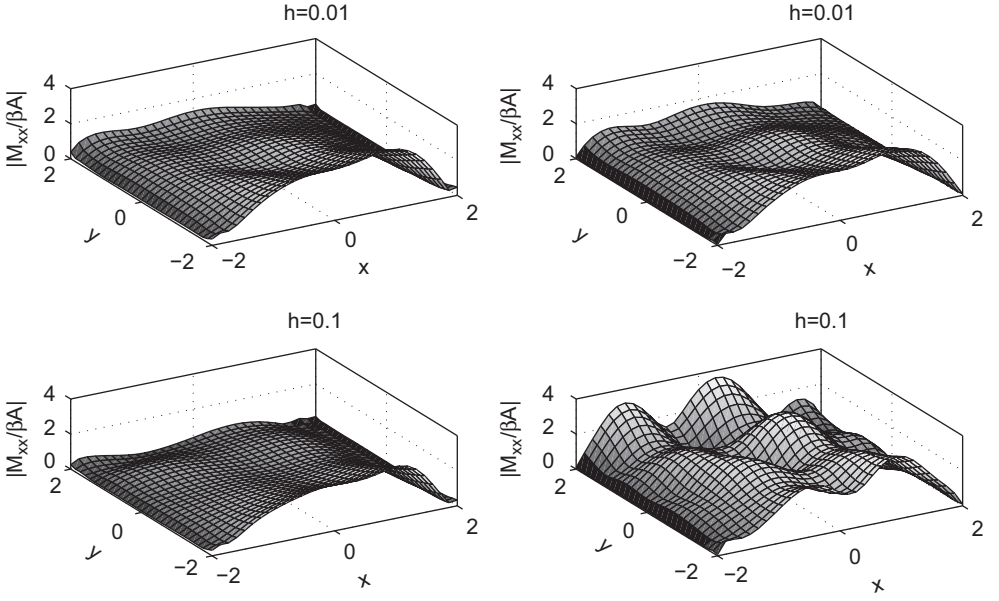

Fig. 4. Comparison of bending moments M_{xx} calculated using method M (left) and method K (right) for the indicated plate thickness. Plate and water properties are the same as in Fig. 3.

that of method K since the condition imposed on the plate rotations in the Mindlin plate theory is less stringent than the Kirchhoff plate theory. However, as $h \to 0$, the solutions converge to each other, as discussed below.

We now compare the moments and shear forces for methods K and M. For method K, the moments and shear forces involve the second and the third derivatives of the displacement w. In order to 'match' the moments and shear forces calculated using method M, we use the same number of elements for both methods. However, despite agreeing on displacements, the moments and shear forces calculated using method K are inaccurate. This inaccuracy is shown in Figs. 4–6, where the moments and shear forces of the plate with the same parameters as in Fig. 3 are calculated for $h = 0.01$ and 0.1 using methods K and M. The moments from both methods, as shown in Figs. 4 and 5, only agree for a relatively small thickness $h = 0.01$. However, for a thicker plate, the moments and forces from method K begin to diverge from those given by method M; in particular, the solutions from method K lose the smoothness that is required

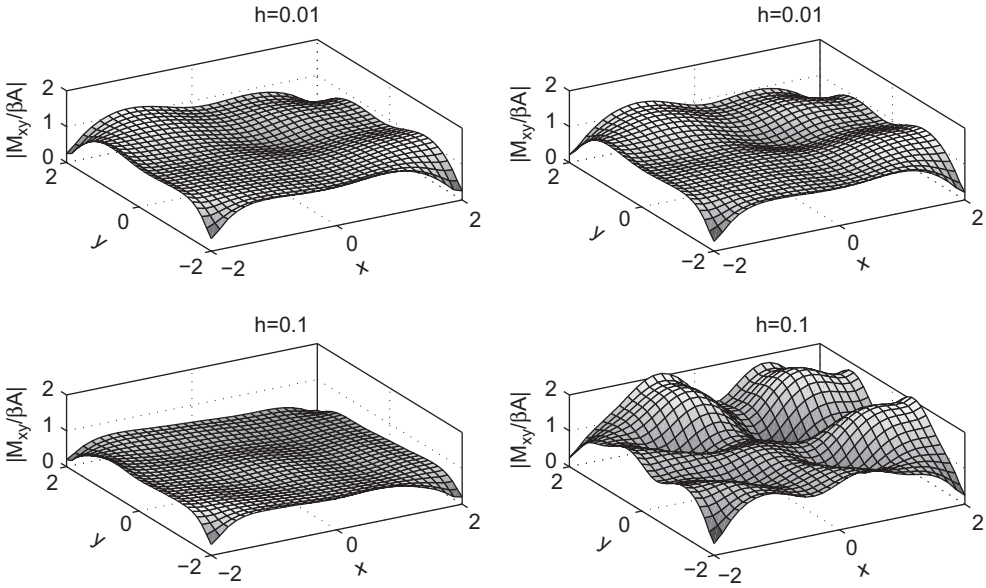

Fig. 5. Caption the same as Fig. 4 except for twisting moment M_{xy}.

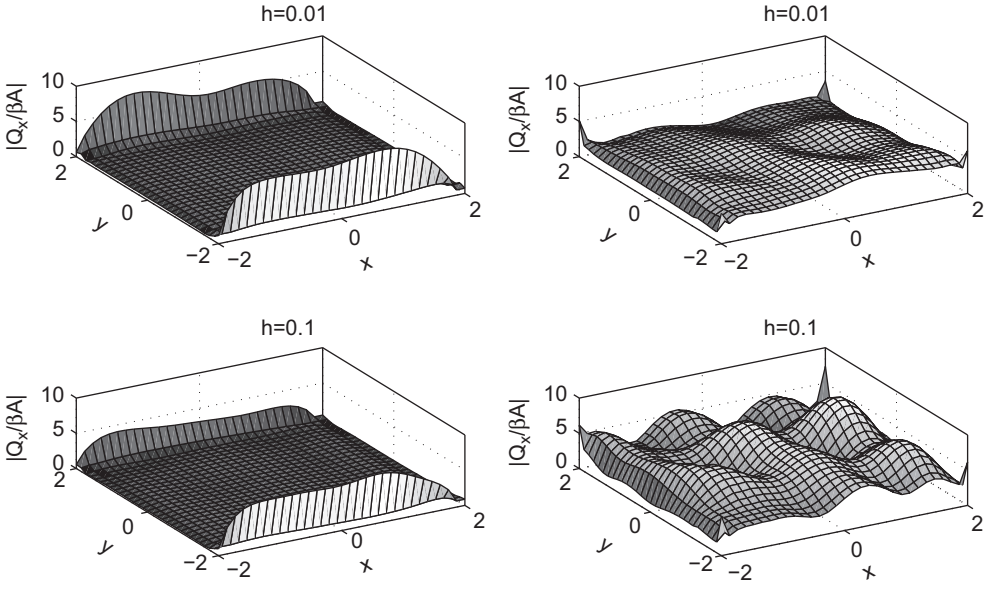

Fig. 6. Caption the same as Fig. 4 except for shear force Q_x.

since the moments and shear forces are continuous functions. As shown in Fig. 6, the shear forces from method K are erroneous. This problem has been addressed in Wang et al. (2001).

To understand the degree of similarity between methods K and M, we vary the discretisation size in method M and check whether the displacement, moments, and shear forces converge to the results from method K as $h \to 0$. We take the element size to be proportional to the wavelength. This is so that we can capture the oscillation of the waves as well as the plate. For a square plate, we relate the element-length characteristic a to the wavelength λ by the equation

$$a = c\lambda, \tag{54}$$

where $0 < c < 1$ is the constant of proportionality.

For the comparison of methods M and K, relative error $\varepsilon(f)$ is defined as

$$\varepsilon(f) = \int_{\Delta} \frac{|f^{(M)} - f^{(K)}|}{|f^{(K)}|}\, \mathrm{d}A, \tag{55}$$

where f can be w, M_{xx}, M_{xy}, or Q_x and the superscript indicates the method used. We assume that results computed using method K with $c = \frac{1}{25}$ are sufficiently close to the actual solution and use this as a reference. The plate thickness h is taken to be 0.1, 0.01 and 0.001 and the mass constant is set to be $\gamma_1 = h$ with $\gamma_2 = \frac{1}{12}h^2\gamma_1$. Tables 2–4 show that the displacement, bending moments, and twisting moments of method M converge to the solutions of method K as we decrease the thickness h. However, since the shear forces computed by method K are incorrect, we see large errors in Table 5. Moreover, by comparing columns corresponding to $h = 0.01$ and 0.001, we notice that the errors in the moments M_{xx} and M_{xy} are rather similar. This is because the results for $h = 0.01$ and 0.001 are very close to each other. Therefore, $h = 0.01$ might be said to be the limit before which the plate thickness becomes significant.

4.2. Results for displacement, moments, and shear forces in a rectangular plate

We present the results for a rectangular plate of area $4LB = 16$ with $L/B = 2$ (i.e. $L = 2\sqrt{2}$ and $B = \sqrt{2}$). The results are computed using method M for two different plate thickness $h = 0.01$ and 0.1 with water depth $H = 0.5$ (using Eq. (17)) and $H \to \infty$ (using Eq. (18)). We adopt the stiffness constant $\beta = 0.01$, the mass constant $\gamma_1 = h$ and $\gamma_2 = \frac{1}{12}h^2\gamma_1$, the Poisson ratio $\nu = 0.3$, the shear correction factor $\kappa^2 = \frac{5}{6}$, the wavelength $\lambda = 2$, and the waveangle is $\theta = \pi/4$.

Table 2
Relative error $\varepsilon(w)$ of displacements computed by methods M and K

c	Number of elements	h		
		0.1	0.01	0.001
$\frac{1}{5}$	100	1.1902×10^{-1}	3.4477×10^{-2}	2.8220×10^{-2}
$\frac{1}{10}$	400	1.1814×10^{-1}	1.6568×10^{-2}	7.2455×10^{-3}
$\frac{1}{15}$	900	1.1822×10^{-1}	1.3929×10^{-2}	3.2864×10^{-3}
$\frac{1}{20}$	1600	1.1824×10^{-1}	1.3193×10^{-2}	2.2222×10^{-3}
$\frac{1}{25}$	2500	1.1825×10^{-1}	1.2880×10^{-2}	1.8743×10^{-3}

Table 3
Relative error $\varepsilon(M_{xx})$ of bending moments computed by methods M and K

c	Number of elements	h		
		0.1	0.01	0.001
$\frac{1}{5}$	100	1.5789×10^{-1}	9.4177×10^{-2}	9.5531×10^{-2}
$\frac{1}{10}$	400	1.4852×10^{-1}	5.0502×10^{-2}	5.3258×10^{-2}
$\frac{1}{15}$	900	1.4639×10^{-1}	3.6230×10^{-2}	3.8620×10^{-2}
$\frac{1}{20}$	1600	1.4811×10^{-1}	3.2549×10^{-2}	3.4757×10^{-2}
$\frac{1}{25}$	2500	1.5629×10^{-1}	3.0426×10^{-2}	3.0221×10^{-2}

Table 4
Relative error $\varepsilon(M_{xy})$ of twisting moments computed by methods M and K

c	Number of elements	h		
		0.1	0.01	0.001
$\frac{1}{5}$	100	1.5756×10^{-1}	4.8603×10^{-2}	4.7554×10^{-2}
$\frac{1}{10}$	400	1.3437×10^{-1}	1.7914×10^{-2}	1.9953×10^{-2}
$\frac{1}{15}$	900	1.3377×10^{-1}	1.1548×10^{-2}	1.3624×10^{-2}
$\frac{1}{20}$	1600	1.3453×10^{-1}	9.3821×10^{-3}	1.0755×10^{-2}
$\frac{1}{25}$	2500	1.3525×10^{-1}	8.4957×10^{-3}	9.0843×10^{-3}

Table 5
Relative error $\varepsilon(Q_x)$ of shear forces computed by methods M and K

c	Number of elements	h		
		0.1	0.01	0.001
$\frac{1}{5}$	100	1.0276×10^{0}	6.7120×10^{-1}	6.4788×10^{-1}
$\frac{1}{10}$	400	9.4180×10^{-1}	5.6770×10^{-1}	5.4276×10^{-1}
$\frac{1}{15}$	900	8.8987×10^{-1}	5.1998×10^{-1}	4.9600×10^{-1}
$\frac{1}{20}$	1600	9.0052×10^{-1}	5.2047×10^{-1}	4.9626×10^{-1}
$\frac{1}{25}$	2500	8.8903×10^{-1}	5.0011×10^{-1}	4.7555×10^{-1}

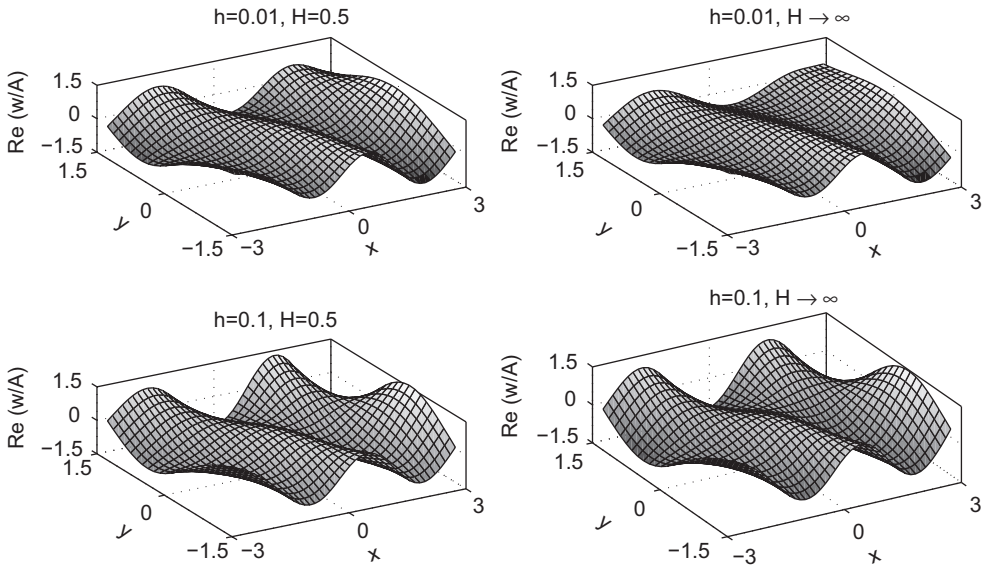

Fig. 7. Real part of the displacement of a rectangular plate of area 16 with $L/B = 2$ and given h.

Figs. 7–10 show the real part of the displacement w/A, the bending moment M_{xx}, the twisting moment M_{xy}, and the shear force Q_x, respectively.

As shown in Figs. 8–10, it may be seen that the maximum values of the stress resultants plotted are increasd in the shallower water case. However, it should be noted that the difference in the plate thicknesses significantly affects the response, in particular, in terms of the moments and shear forces. This shows that it is important to account the plate thickness to obtain accurate results, in particular of moments and shear forces.

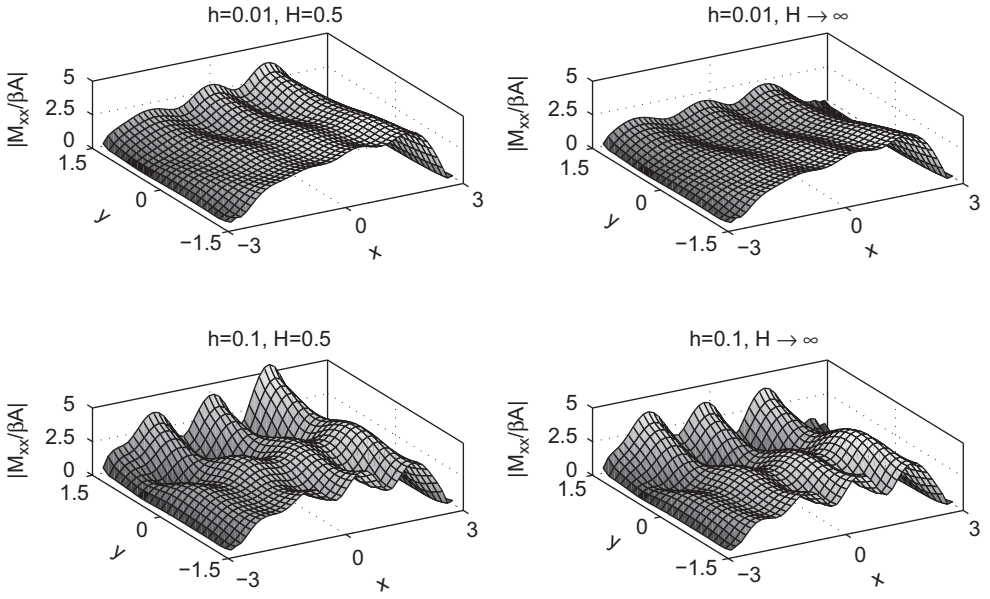

Fig. 8. Absolute value of the bending moment M_{xx} for the same configuration as Fig. 7.

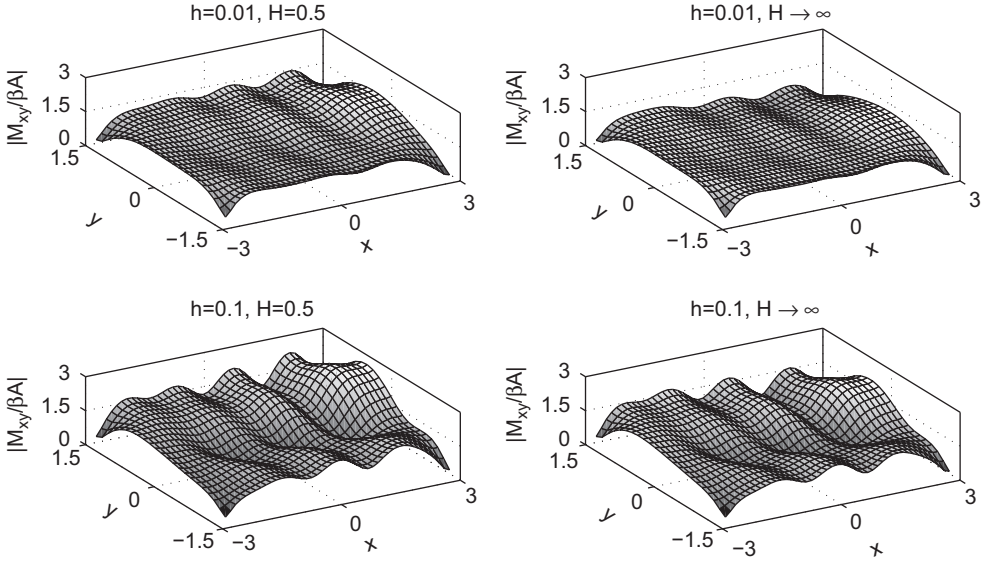

Fig. 9. Absolute value of the twisting moment M_{xy} for the same configuration as Fig. 7.

5. Conclusion

Motivated by the need to obtain accurate stress resultants for checking the strength and for design purposes, we have developed a method for computing hydroelastic responses of a floating elastic plate using the Mindlin plate theory. This theory is chosen because it accounts for the effects of transverse shear deformation and rotary inertia of the plate, which are neglected in the Kirchhoff plate theory. These effects can be substantial in certain cases, for example high frequency waves (short wavelengths as compared to the characteristic length of the floating structure—a feature of VLFS). Moreover, in the Kirchhoff plate theory, the three free-edge boundary conditions are too many, and are thus reduced to two by imposing that the sum of $\partial M_{ns}/\partial n$ and Q_n is zero. These are unchanged in the Mindlin plate theory. Another reason for using the Mindlin plate theory is that the stress resultants depend, at most, on the first derivatives of the plate

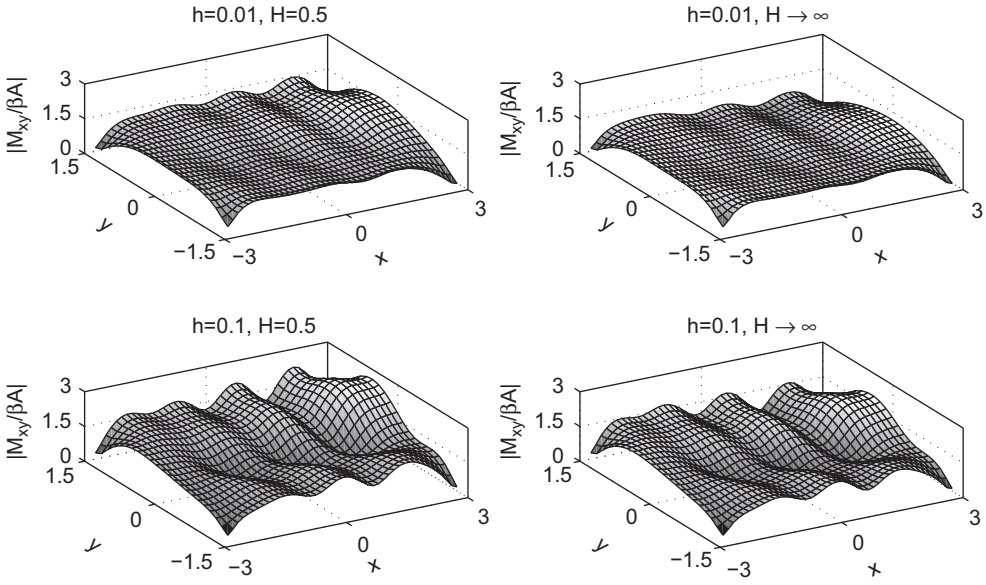

Fig. 10. Absolute value of the shear force Q_x for the same configuration as Fig. 7.

displacement and rotations, unlike the Kirchhoff plate theory which depends on the third derivatives of the displacement.

Mathematically, unlike the Kirchhoff plate theory where the plate motion is governed by a biharmonic equation acting on the displacement, the Mindlin plate theory uses three simultaneous equations involving the displacement as well as two rotations about the x and y axes. However, the conventional way of coupling the plate and the water motion using a hybrid FE–BE method, e.g. Wang and Meylan (2004), is still applicable, that is by solving the plate motion using the FEM through the variational equation for the plate and then solving the integral equation representing the water velocity potential using the FEM shape function. In this case we chose a four-node linear serendipity shape function for a rectangular element. Yet it must be noted that the chosen shape function gives inaccurate approximation of the strain functions. Therefore, the strain must be obtained by interpolating it around the edges of the rectangular element. We compared the results with the known ones from Wang and Meylan's FE–BE method with a thin plate. Though the displacements agreed well between the two methods, the moments agreed less as h increases. Moreover, the shear forces of both methods did not agree. This reflects the limitation of method K in calculating the moments and shear forces for thicker plate.

The present method can be improved in several ways. One is to use quadrilateral elements instead of restricting the elements to rectangles, and thus allowing the elements to fit the shape a plate of arbitrary geometry. Rectangular elements are restricted at the edge of the plate and, hence, fails to satisfy the specified boundary conditions imposed on the moments and shear forces. The method can also be improved by choosing a higher-order shape function, e.g. based on eight-noded elements.

References

Abramowitz, M., Stegun, I., 1964. Handbook of Mathematical Functions. Dover Inc., New York.

Bathe, K.-J., Dvorkin, E.N., 1985. Short communication: a four-node plate bending element based on Mindlin/Reissner plate theory and a mixed interpolation. International Journal for Numerical Methods in Engineering 21, 367–383.

Hermans, A.J., 2000. A boundary element method for the interaction of free-surface waves with a very large floating flexible platform. Journal of Fluids and Structures 14, 943–956.

Kashiwagi, M., 1998. A B-spline Galerkin scheme for calculating hydroelastic response of a very large floating structure in waves. Journal of Marine Science and Technology 3, 37–49.

Kashiwagi, M., 2000. Research on hydroelastic response of VLFS: recent progress and future work. International Journal of Offshore & Polar Engineering 10, 81–90.

Kirchhoff, G., 1850. Über das Gleichgewicht und die Bewegung einer Elastischen Scheibe. Journal für de Reine und Angewandte Mathematik 40, 51–58.

Landesman, E.M., Hestenes, M.R., 1992. Linear Algebra for Mathematics, Science and Engineering. Prentice-Hall, New Jersey.
Liew, K.M., Xiang, Y., Kitipornchai, S., 1993. Transverse vibration of thick rectangular plates—I. Comprehensive sets of boundary conditions. Computer & Structures 49, 1–29.
Liew, K.M., Wang, C.M., Xiang, Y., Kitipornchai, S., 1998. Vibration of Mindlin Plates—Programming the p-Version Ritz Method. Elsevier Science Ltd., The Netherlands.
Linton, C.M., 1999. Rapidly convergent representation for Green's function for Laplace's equation. Proceedings of the Royal Society of London A 455, 1767–1797.
Liu, W.K., Zhang, Y., Ramirez, M.R., 1991. Multiple scale finite element methods. International Journal for Numerical Methods in Engineering 32, 969–990.
Mei, C.C., 1982. The Applied Dynamics of Ocean Surface Waves—Advanced Series on Ocean Engineering. World Scientific, Singapore.
Meylan, M.H., 2002. The wave response of ice floes of arbitrary geometry. Journal of Geophysical Research—Oceans 107 (C1), 1–15.
Mindlin, R.D., 1951. Influence of rotary inertia and shear on flexural motions of isotropic elastic plates. Journal of Applied Mechanics 18, 31–38.
Squire, V.A., Duggan, J.P., Wadhams, P., Rottier, P.J., Liu, A.J., 1995. Of ocean waves and sea ice. Annual Review of Fluid Mechanics 27, 115–168.
Stoker, J.J., 1957. Water Waves. Interscience Publishers Inc., New York.
Tayler, A.B., 1986. Mathematical Models in Applied Mathematics. Clarendon Press, Oxford.
Utsunomiya, T., Watanabe, E., Eatock Taylor, R., 1998. Wave response analysis of a box-like VLFS close to a breakwater. In: 17th International Conference on Offshore Mechanics and Arctic Engineering, ASME, OMAE98-4331, pp. 1–8.
Wang, C.D., Meylan, M.H., 2004. A higher order method for the wave forcing of a floating thin plate of arbitrary geometry. Journal of Fluids and Structures 19, 557–572.
Wang, C.M., Xiang, Y., Utsunomiya, T., Watanabe, E., 2001. Evaluation of modal stress resultants in freely vibrating plates. International Journal of Solids and Structures 38, 6525–6558.
Watanabe, E., Utsunomiya, T., Wang, C.M., 2004. Hydroelastic analysis of pontoon-type VLFS: a literature survey. Engineering Structures 26, 245–256.
Watanabe, E., Utsunomiya, T., Wang, C.M., 2006. Benchmark hydroelastic responses of a circular VLFS under wave action. Engineering Structures 28, 423–430.
Wehausen, J., Laitone, E., 1960. Surface waves. In: Handbuch der Physik, Fluid Dynamics III, vol. 9. Springer, Berlin.
Zienkiewicz, O.C., 1977. The Finite Element Method, third ed. McGraw-Hill, London.